1967-09-05

Collision Spectroscopy. I. analysis of the scattering of He+ by Ne and Ar

Smith, F.T.

American Physical Society

Physics Review A, v.161, no.1 September 5, 1967, pp. 31-46

http://hdl.handle.net/10945/47763

since r_0 is arbitrary. Due to antisymmetry the first equation in (6.8) gives only one relation, which corresponds to the continuity of z at $r=r'$. The second equation gives 4 relations, of which only 3 are independent of the first equation, which include the smoothness of z' and the proper jump condition on g' at $r=r'$.

The noniterative determination of g for a potential containing two nonlocal components, one separable and the other a Green's function, can be considered an extension of the techniques used by Yamanouchi, Percival, and Marriot for the noniterative determination of a wave function for such nonlocal interactions. G^P could in fact have been obtained somewhat more directly by first rewriting (1.1) in the form of coupled equations, analogous to (6.4), and then considering the regular and irregular wave function solutions of the coupled homogeneous equations.

For the case of $L=0$, $\epsilon=-1$, the second term in the right-hand side (rhs) of (6.2) can be shown to cancel the effect of the first term in the rhs of (6.1). Thus one obtains g by simply dropping the $(E-2E_{T0})rr'$ term in g_2 and the $(E-2E_{T0})r$ term in $w_{22}^{(0)}$, and also dropping the second term in the rhs of (6.2).

One of us (L.S.) would like to express his warm thanks to Dr. Mittleman for his original suggestion that the equation for g could be decoupled, so that it should be possible to write g as a sum of products, and for some helpful comments.

PHYSICAL REVIEW VOLUME 161, NUMBER 1 5 SEPTEMBER 1967

Collision Spectroscopy. I. Analysis of the Scattering of He^+ by Ne and Ar†

F. T. SMITH, R. P. MARCHI, W. ABERTH, AND D. C. LORENTS
Stanford Research Institute, Menlo Park, California
AND
O. HEINZ
Naval Postgraduate School, Monterey, California

(Received 19 April 1967)

Experimental data on the differential scattering of He^+ by Ne and Ar in the energy range from 10 eV to 100 keV are plotted in a reduced coordinate system suggested by a scaling law for the forward scattering. The resulting curves are used to determine the interaction potential. The repulsive interaction dominating at higher energies shows pronounced shell-structure effects, leading to the deduction of the screening constants for the L and M shells of Ar and for the K and L shells of Ne. At lower energies a polarization attraction appears, allowing deduction of the polarizabilities of Ne and Ar. A simple analytic potential is constructed, including a polarizability term appropriately damped inside the outer shell, which fits the data over the entire range. In addition to the pure elastic scattering, effects of inelastic interactions are diagnosed. A prominent curve crossing is located and the scattering pattern arising from it is interpreted by a semiclassical theory. In collisions with closer encounters, a different type of inelastic process appears which apparently involves a more intense coupling than the curve crossing and which appears to open up a number of competing inelastic channels.

I. INTRODUCTION

THE connection between the electronic states of a diatomic system and its collision properties is best studied in differential scattering where the large amount of available information provides a stringent test of our theoretical understanding. Such experiments are now producing a growing mass of data of spectroscopic quality which deserve detailed interpretation. These data can be used to test predictions derived from prior theoretical knowledge about the electronic states of the system, but it is also possible to deduce a great deal of information about these states empirically from an analysis of the scattering spectra. It is to such an analysis that this paper is devoted.

Symmetric systems provide the most information because of the structure in the interference patterns that arise in them. For example, in the system He^++He, oscillations appear in the elastic scattering pattern due both to electronic symmetry (g and u states) and nuclear symmetry.[1] These oscillations can be used to deduce detailed empirical information about potentials for the states involved. Similarly, in Ne^++Ne, Jones[2] has observed an additional symmetry effect due to participation of Π as well as Σ states in the scattering. Most theoretical information on the potentials is available for symmetric systems with 4 or fewer elec-

† Supported in part by the National Aeronautics and Space Administration and by the U.S. Army Research Office.

[1] R. P.Marchi and F. T. Smith, Phys, Rev. **139**, A1025 (1966); W. Aberth, D. C. Lorents, R. P. Marchi, and F. T. Smith, Phys. Rev. Letters **14**, 776 (1965).

[2] P. R. Jones, T. L. Batra, and H. A. Ranga, Phys. Rev. Letters **17**, 281 (1966).

trons. For experimental reasons, He^++He has been studied in greater detail than the others, and even this 3-electron system has not been fully explored.

In asymmetric systems, on the other hand, inelastic processes are emphasized, since such processes as charge transfer, for instance, can no longer occur elastically. Because of the lower symmetry of these systems, the potential energy curves take a different form and certain interactions between them are allowed which are forbidden in symmetric systems. Except for H^++He and its companion He^++H, which have been studied experimentally by Everhart and co-workers,[3] the potential-energy curves have not been studied in much detail for the asymmetric systems most readily accessible to experimental study. Thus, the study of asymmetric systems provides a valuable testing ground for our abilities to deduce information about the electronic states purely from the scattering data. It is from this point of view that we have attempted a thorough analysis of the data on scattering of He^+ by Ne and Ar,[4] since these data provide us with a good deal of information about some of the low-lying potential curves for these systems.

The principal tool that we have used in the analysis of the differential scattering experiments is a recently developed approximate scaling law for forward scattering.[5] The experimental data in differential scattering are naturally a function of at least two variables, the angle of scattering and the energy. Because of experimental limitations, cross sections are available at any given energy only over a limited range of angles. The scaling law is important because it allows us to compile into one picture data taken at widely varying energies, in our case from 10 to 100 000 eV. These data were obtained at two laboratories using different techniques and thus provide an interesting test of the value of the scaling procedure.

The results of the analysis we report here greatly exceed our initial expectations. We are convinced that differential scattering is a potent tool for probing atomic interactions both in the outer, chemically active, shells and in the inner core. The resulting spectra show much detailed structure, comparable to the details seen in optical spectroscopy or in mass spectra, and even more closely analogous to those seen in nuclear scattering. These features can be interpreted quantitatively to provide much information about the potentials and interactions of the electronic states of the colliding diatomic system. We hope to see a rapid development of the resulting collision spectroscopy.

[3] Herbert F. Helbig and Edgar Everhart, Phys. Rev. **136,** A674 (1964).

[4] W. Aberth and D. C. Lorents, Phys. Rev. **144,** 109 (1966); P. R. Jones, F. P. Ziemba, H. A. Moses, and E. Everhart, *ibid.* **113,** 182 (1959); E. N. Fuls, P. R. Jones, F. P. Ziemba, and E. Everhart, *ibid.* **107,** 704 (1957).

[5] Felix T. Smith, R. P. Marchi, and Kent G. Dedrick, Phys. Rev. **150,** 79 (1966).

II. THEORETICAL CONSIDERATIONS

The Scaling Principle

The experimental data in differential scattering are usually presented in terms of the differential cross section $\sigma(\theta, E)$ as functions of the experimental variables angle and energy (we shall always assume that the conversion to center-of-mass variables has been made). In computing this functional relationship from the interaction potential, the impact parameter b plays a prominent part, although it is not actually observable in scattering experiments. It has been recognized for some time that the quantity $\tau = E\theta$ in small-angle forward scattering is primarily a function of the impact parameter, and Lehmann and Leibfried[6] have shown that this is a consequence of the fact that τ can be expressed as a power series in the reciprocal energy in which the coefficient of each term is a function of b alone:

$$\tau(E, b) = E\theta = \tau_0(b) + E^{-1}\tau_1(b) \cdots . \tag{1}$$

The first term in this series is

$$\tau_0(b) = -b \int_b^\infty \left(\frac{dV}{dr}\right) \frac{dr}{(r^2 - b^2)^{1/2}}. \tag{2}$$

By inverting the function (1), we obtain b as a function of τ and E, and this in turn can be written as an expansion of the same sort:

$$b(\tau, E) = b_0(\tau) + E^{-1}b_1(\tau) \cdots . \tag{3}$$

From the usual expressions for the differential cross section, it is then easy to see that an appropriate reduced cross section which is expandable in like manner can be constructed as follows:

$$\rho(\tau, E) = \theta \sin\theta\sigma(\theta, E)$$
$$= \tfrac{1}{2} \left| \partial b^2/\partial \ln\tau \right| = \rho_0(\tau) + E^{-1}\rho_1(\tau) \cdots . \tag{4}$$

The scaling principle $\rho(\tau, E) \approx \rho_0(\tau)$ for small angle scattering follows immediately if one omits all but the leading term in the series of Eq. (4). The advantages of using this scaling principle are obvious. Differential cross sections obtained at various energies and angles, when plotted in a reduced form (i.e., ρ versus τ), yield a single curve.[7] This produces an immediate indication of the precision of the experiments and it also greatly simplifies the inversion procedure. Furthermore, features that occur at the same value of τ for different energies indicate that they originate at a common region of the interaction potential, since constant τ

[6] C. Lehmann and G. Leibfried, Z. Physik **172,** 465 (1962).

[7] It appears that the function $\rho_1(\tau)$ vanishes fairly rapidly at small values of τ; the consequence is that the scaling principle is useful at small enough angles even at quite low values of the energy, but naturally as the angle is increased the reduced cross section $\rho(\tau, E)$ ultimately deviates from the limiting function $\rho_0(\tau)$. As a result, what seems to be a high-energy expansion turns out really to be a small-angle expansion.

implies nearly constant impact parameter and distance of closest approach. An additional advantage of the scaling principle is that it removes the singular behavior of σ as θ approaches zero, thus permitting easier identification of abnormal behavior at small angles.

Since we shall ultimately be interested in attempting to construct the potential function from the scattering data, we shall give here the equations that can be employed. By integrating the first term of Eq. (4), we obtain an estimate of the impact parameter as a function of τ:

$$b_0^2(\tau) = 2\int_\tau^\infty \rho_0(\tau')\, d\ln\tau'. \tag{5}$$

From this it is easy to obtain an empirical reduced deflection function $\tau_0(b)$, and the potential can then be obtained by an integration:

$$V(r) = \frac{2}{\pi}\int_r^\infty \frac{\tau_0(b)\, db}{(b^2 - r^2)^{1/2}}. \tag{6}$$

This method of obtaining a potential is related to the procedure introduced by Firsov and used by Everhart[8] and his colleagues, but it has the advantage of making use in one expression of data from a number of different energies. Of course, it is often possible to avoid full use of these inversion equations by fitting parameters in an assumed analytical form for the potential $V(r)$ or the reduced deflection function $\tau_0(b)$.

III. TREATMENT OF THE EXPERIMENTAL DATA

1. General

The most detailed information on the elastic scattering of He^+ by Ne and Ar is that of Aberth and

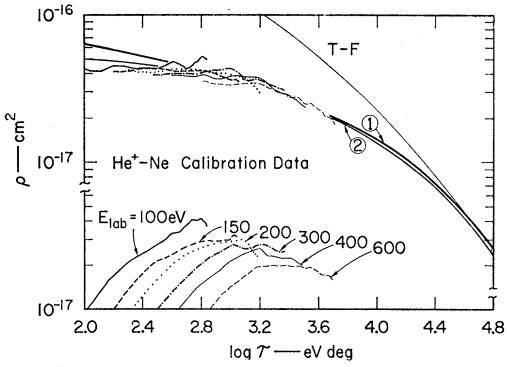

FIG. 1. Reduced cross sections from the absolute (calibration) measurements on the scattering of He^+ by Ne. The lower curves show the original data. The upper curves show the data with a correction for angular resolution. Three theoretical curves are shown. T–F is the one corresponding to the Thomas-Fermi model. ① is a one-term screened Coulomb potential. ② is a two-term screened Coulomb with polarization attraction. (The base of the logarithm is 10.)

[8] G. H. Lane and E. Everhart, Phys. Rev. **120**, 2064 (1960).

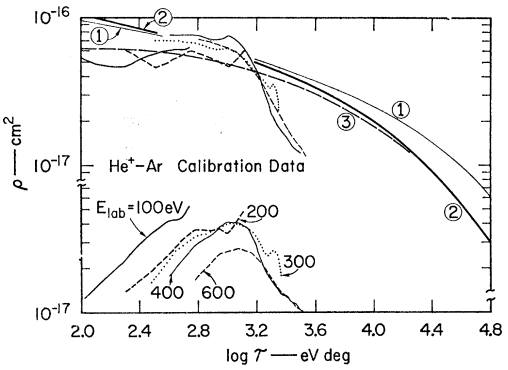

FIG. 2. Reduced cross sections from the absolute (calibration) measurements on the scattering of He^+ by Ar. The lower curves show the original data. The upper curves show the data with a correction for angular resolution. Three theoretical curves are shown. ① represents a one-term screened Coulomb interaction. ② represents a two-term screened Coulomb interaction. ③ represents the three-term screened Coulomb with a polarization attraction. (The base of the logarithm is 10.)

Lorents.[4] Their original data have been replotted and are presented as logarithmic plots of ρ against τ in Figs. 1 through 6. In order to compile all the data together for Figs. 3 and 4, we averaged the information from all the runs at each energy. Since different intervals were used in tabulating the data from different runs, it was often necessary to interpolate before averaging, and a 4-point Lagrange interpolation was used. The averaging was then done with the data from each run weighted by the number of points measured in that run.

The data of Aberth and Lorents were taken at laboratory energies from 10 to 600 eV. In addition, Everhart and his colleagues[3] have published measurements on the same systems at much higher energies, namely, from 25 to 100 keV. They did not measure the elastic scattering, but they provide information on the total scattering independent of charge and energy loss at each angle and they also measured the fractions of this total associated with charges 0, +1, and +2. We have replotted their data in the reduced coordinates using only the total values, i.e., the scattering independent of charge. At the high energies covered by these experiments, this cross section is a good representation of the quasielastic scattering that is the simplest to understand. At these energies, scattering at only a few degrees involves very penetrating encounters with small impact parameters, and the deflection experienced by the heavy nuclei is governed by the interaction mainly in the innermost region largely inside the electron clouds, where the potential approximates a simple screened-Coulomb form. On the other hand, the charge distribution when the particles finally separate depends on interactions between the outer electrons which remain important at internuclear distances comparable to the Bohr length a_0 and so is fairly independent of the forces which control the nuclear scattering.

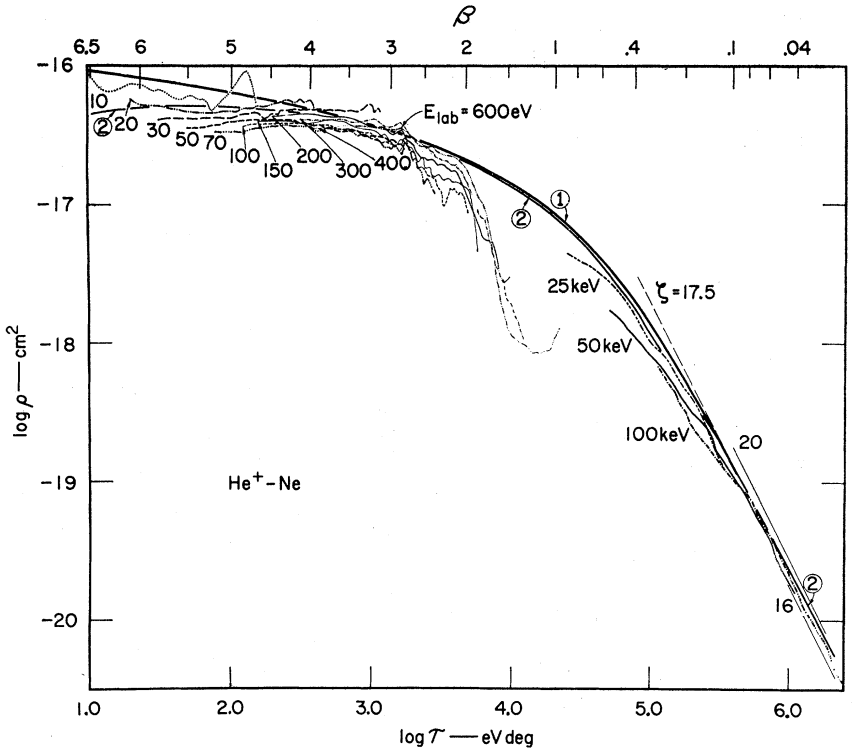

FIG. 3. Reduced plot of the pure elastic-scattering data in He^++Ne at energies from 10 to 600 eV, together with the quasielastic scattering data of Everhart *et al.* from 25 to 100 keV. The elastic-scattering data are relative measurements calibrated against the data of Fig. 1. The theoretical curves marked ① and ② are the same as those of Fig. 1. In addition, we show the limiting straight lines for pure coulomb scattering with several values of the effective nuclear-charge parameter $\zeta=Z_1Z_2$. The reduced impact parameter β is shown at the top of the figure. (The base of the logarithms is 10.)

Everhart and his co-workers indeed observed significant, though gradual, variation of the charge ratios as a function of angle, but these ratios clearly depend on E as well as τ, and we suspect that more details of their energy dependence are needed before it will be possible to analyze their behavior in detail. Since we are interested mainly in the interaction potentials responsible for the scattering, we have ignored these charge ratios here.

In Figs. 3 and 4 we present the combined data of Aberth and Lorents on the low-energy elastic scattering and the data of Everhart and his colleagues on high-energy quasielastic scattering.

In addition to the elastic and quasielastic scattering data, a certain amount of information on inelastic scattering has been obtained in two ways. Aberth and Lorents measured energy-loss spectra at a few angles in the course of their experiments. Despite relatively poor energy resolution, these spectra show some interesting structure. Novick[9] and his co-workers have recently observed the optical spectra excited by charge-transfer collisions at fairly low energies in the same systems. These observations provide additional information which should ultimately be incorporated in a consistent picture of the scattering processes.

2. Small-Angle Behavior

The experimental data of Lorents and Aberth, when originally plotted in the reduced coordinates ρ versus τ, showed a decided falloff at small angles at each energy. This feature is clearly due to deteriorating angular resolution of their rectangular slit system as $\theta\rightarrow 0$. In the lower part of Figs. 1 and 2 we show examples of this behavior in the data from the calibration runs for He^++Ne and He^++Ar, in which the cross sections were measured absolutely. In their falloff at low angles the successive curves are strikingly parallel to each other, and the same feature appears in the rest of the data for both target gases. This appears to be a happy by-product of the fact that the reduced cross section $\rho(\tau, E)$ becomes almost constant at small τ except near a "rainbow" feature.

In view of the finite angular resolution, the experimental cross section really represents an average over a range of angles near θ. We may express the averaging symbolically through the distribution function $f(\theta, \Delta\theta)$, recognizing that $\Delta\theta$ may really stand for several degrees of freedom in the geometry of the laboratory measurements. Because of the small-angle connection between

[9] M. Lipeles, R. Novick, and N. Tolk, Phys. Rev. Letters 15, 815 (1965).

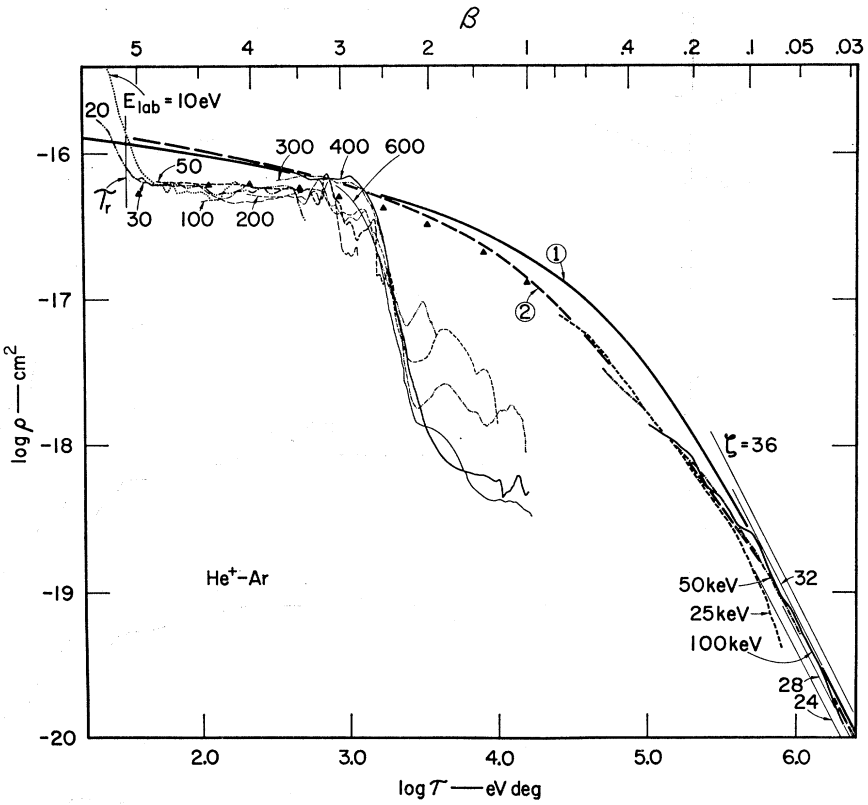

FIG. 4. Reduced plot of the pure-elastic-scattering data in He^++Ar at energies from 10 to 600 eV, together with the quasi-elastic scattering data of Everhart *et al.* from 25 to 100 keV. The elastic-scattering data are relative measurements calibrated against the data of Fig. 1. The theoretical curves marked ① and ② are the same as those of Fig. 2. The solid triangles represent curve ③ from Fig. 2. The location of the rainbow is shown at τ_r. In addition, we show the limiting straight lines for pure Coulomb scattering with several values of the effective-nuclear-charge parameter $\zeta=Z_1Z_2$. The reduced impact parameter β is shown at the top of the figure. (The base of the logarithms is 10.)

σ and ρ,

$$\rho(E\theta, E)\cong\theta^2\sigma(\theta, E), \tag{7}$$

it is easy to see that

$$\rho_{\text{expt}}(E\theta, E)$$

$$=\theta^2\int\sigma(\theta+\Delta\theta, E)f(\theta, \Delta\theta)\,d\Delta\theta$$

$$=\int\rho[E(\theta+\Delta\theta), E](1+\Delta\theta/\theta)^{-2}f(\theta, \Delta\theta)\,d\Delta\theta. \tag{8}$$

As long as ρ is a slowly varying function of τ (and E), we can take it outside the integral (to be more sophisticated, we could expand ρ in Taylor's series about $E\theta$), with the result

$$\rho_{\text{expt}}(E\theta, E)\cong\rho_0(E\theta)\,J(\theta), \tag{9}$$

where

$$J(\theta)=\int(1+\Delta\theta/\theta)^{-2}f(\theta, \Delta\theta)\,d\Delta\theta. \tag{10}$$

The function $J(\theta)$ can be evaluated approximately by comparing the experimental curves with each other. The resulting function can be used as an empirical correction to the experimental curves.

The transition from Eqs. (8) to (9) is of course legitimate only where $\rho_0(\tau)$ is slowly varying, and not where it is changing rapidly as it does in a rainbow region. In such a case the use of the correction function $J(\theta)$ is not really justified. The same thing is true in symmetric scattering (e.g., He^++He), where $\rho(\tau, E)$ oscillates rapidly. In the asymmetric cases under examination here, the experimental results show that $\rho(\tau)$ varies slowly over most of its course, and we have therefore been able to apply a single instrumental correction to the data for both target gases, Ne and Ar.

The best simple empirical form we could find for $J(\theta)$ was

$$\log_{10}J(\theta)=-B/\theta. \tag{11}$$

Qualitatively, this expresses the behavior to be expected when the rectangular slits intercept the conical distribution of scattered ions, the resulting error getting worse as the angle of the cone decreases. Since the geometry differed between the absolute (calibration) runs and the relative ones, we obtained two values of B:

$$B_{\text{calib}}=0.64°, \qquad B_{\text{rel}}=0.53°. \tag{12}$$

We have applied this correction to all of the data, including the regions of rapid movement in $\rho(\tau)$, but the original data can be recovered if desired by reversing the correction.

In the upper part of Figs. 1 and 2 we show the result of this correction when applied to the absolute calibration data. The resulting curves differ in magnitude only

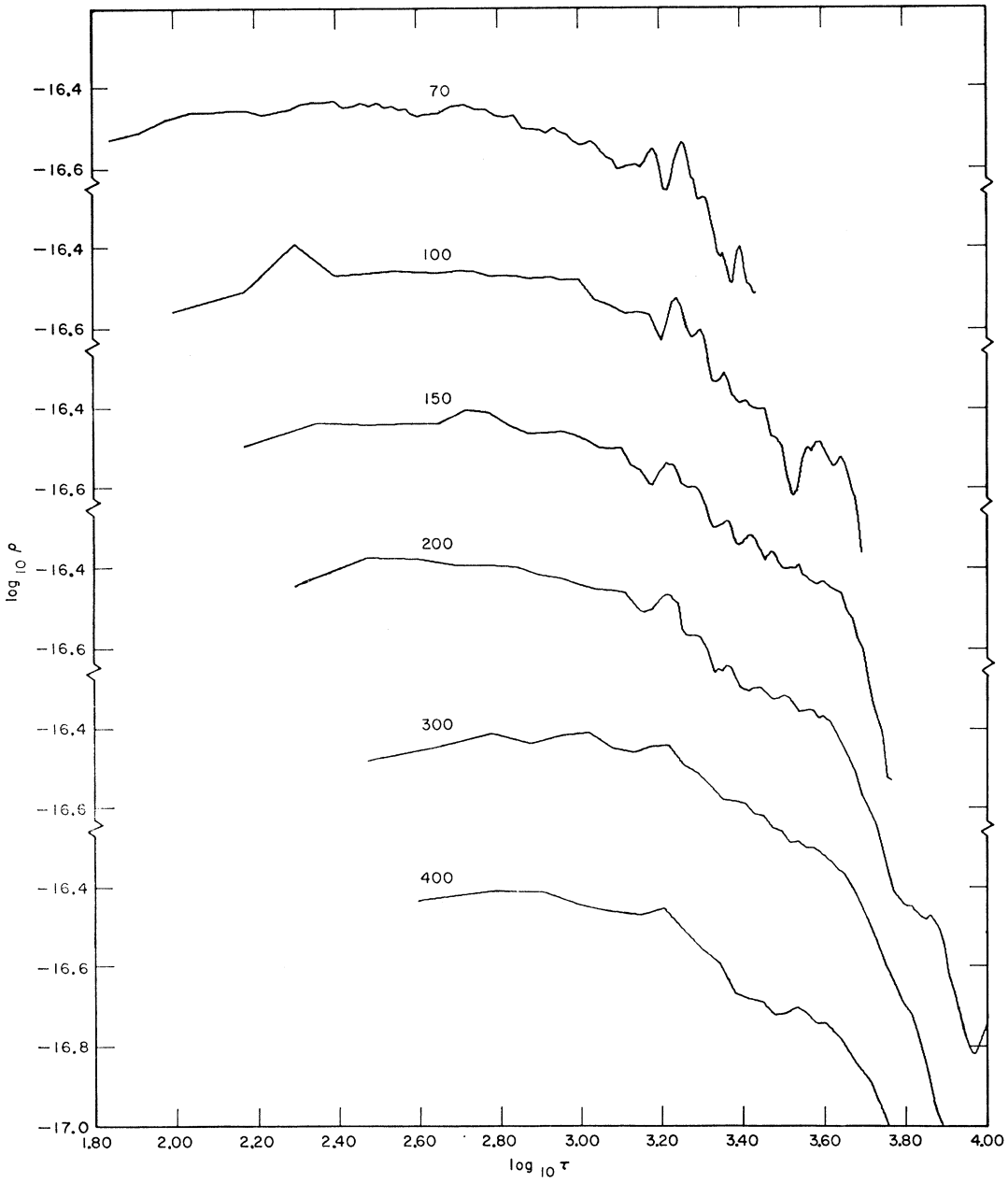

FIG. 5. He^++Ne. Details of the reduced cross section as a function of reduced angle for individual runs at several energies to show the curve-crossing perturbation.

by variations of the size expected from the experimental uncertainties (due largely to the limitations of the pressure measurement), and provide an experimental verification of the validity of the scaling procedure.

The original calibration of the relative data at energies below 100 eV was done by an indirect procedure because absolute measurements were not feasible at lower energies. Instead, the curves were normalized to the 100 eV curves at a constant angle of 3°, assuming that

$$\frac{I(3°, E)}{I(0°, E)} \cdot \frac{I(0°, 100\text{ eV})}{I(3°, 100\text{ eV})} = \frac{\sigma(3°, E)}{\sigma(3°, 100\text{ eV})}, \quad (13)$$

where the I's are measured currents. We now believe that it would be better to normalize the curves to each other by requiring the reduced cross sections ρ to be equal at equal values of τ. Since the scatter among the relative curves as originally normalized is not much

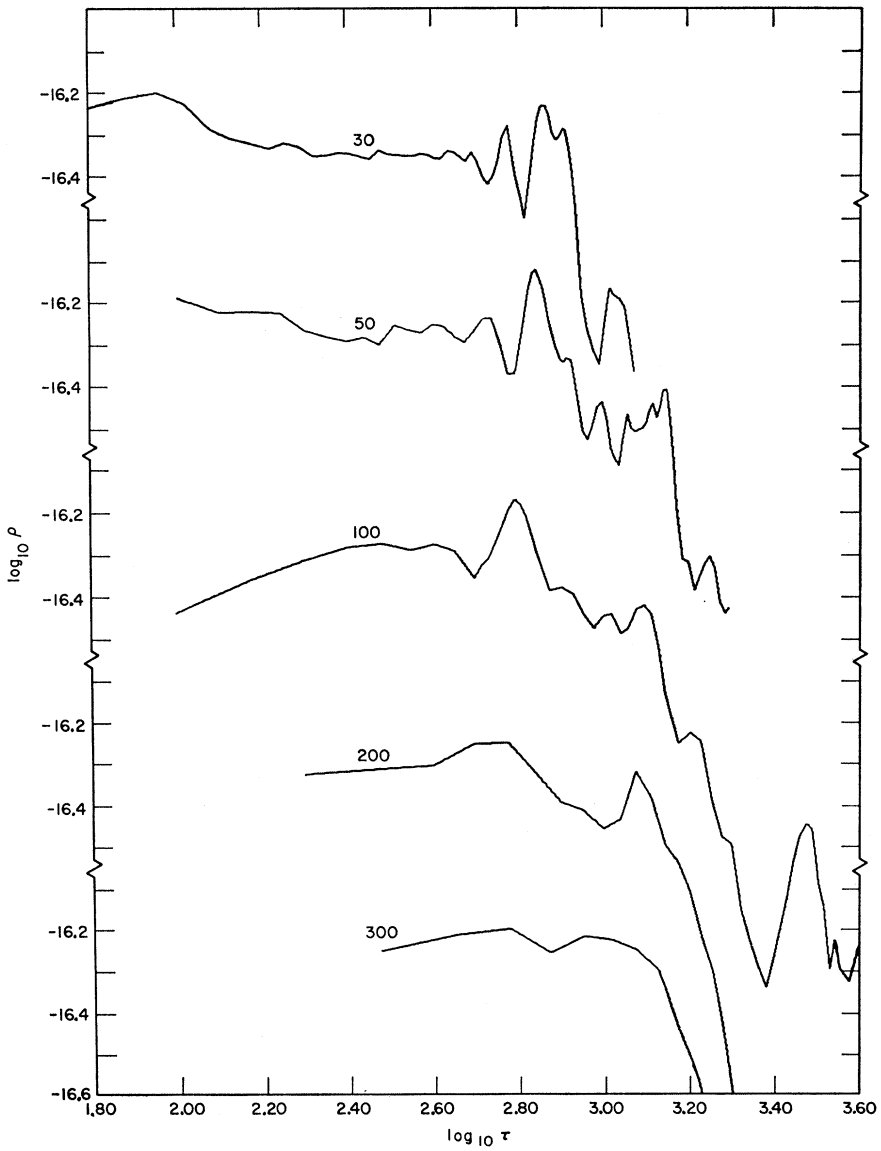

FIG. 6. He^++Ar. Details of the reduced cross section as a function of reduced angle for individual runs at several energies to show the curve-crossing perturbation.

greater than the scatter among the calibration curves, such a recalibration did not seem worth while. For this reason, a methodical trend can be seen in the location of the curves of lowest energies in Figs. 3 and 4 which is probably spurious.

IV. INTERPRETATION OF DATA

1. Principal Features

In Figs. 3 and 4 we have plotted both the low-energy elastic spectra and the quasielastic spectra at high energy due to Everhart and his associates. The data show a gratifying tendency to fall into a single simple pattern in accordance with the expectations aroused by the existence of a scaling law. Several salient features can be observed which we shall discuss in detail in turn.

(a) We observe that the high-energy data appear to fall into a single smooth pattern which approaches a slope of -2 at the right-hand end. The curve can be extrapolated reasonably well to the left to pass through a fairly smooth region approaching the horizontal in the low-energy elastic-scattering data. From this curve we can obtain information on the repulsive potential.

(b) In He^++Ar a steep vertical portion is observed at the extreme left-hand end of the low-energy curves which we attribute to rainbow scattering due to an attractive interaction.

(c) A characteristic structure of peaks and valleys which occurs at constant values of τ at all energies is to

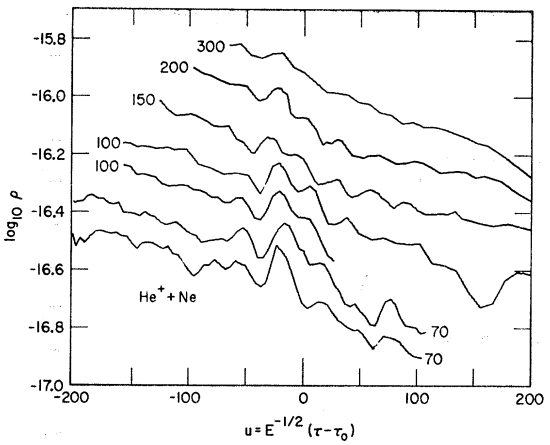

FIG. 7. He^++Ne. Details of the curve-crossing perturbation plotted in the variable u instead of τ to show the proper scaling of the interference oscillations; individual runs are shown separately. The scale on the left applies to the lowest curve and each of the other curves is displaced from its neighbor by 0.1 unit on the scale.

be seen in the elastic-scattering data beginning at $\log_{10}\tau\cong 3.2$ for He^++Ne and at $\log_{10}\tau\cong 2.8$ for He^++Ar. This perturbation of the elastic-scattering pattern we attribute to a prominent curve crossing. It is shown more clearly in Figs. 5 through 8, where data from some individual runs are reproduced.

(d) Toward the right-hand end the elastic-scattering spectra in both cases exhibit a very pronounced and extreme drop, which we attribute to the onset of inelastic processes (including charge transfer). The effect on the elastic scattering is an extensive loss to inelastic channels.

2. The Repulsive Potential

A. The Empirical Fit

In principle it would have been possible to estimate the potential purely numerically by drawing the best smooth curve through the Everhart data and through the elastic data to the left of the region of inelastic losses and using the inversion procedure of Eqs. (5) and (6). The scatter in the data makes such a procedure more ambiguous than would be desired, and we have found it more profitable to attempt to fit the curves using simple, physically plausible, potential functions.

The high-energy data shown in Figs. 3 and 4 were previously used by Lane and Everhart[8] to obtain an estimate of the potentials by the use of Firsov's method. They obtained separate potentials from the data at each energy. However, as the reduced plots of Figs. 3 and 4 show, these data are entirely consistent from energy to energy, the scatter between them never exceeding about 30% and usually being far less. At the right-hand end these curves approach a slope of -2, which is to be expected for pure Coulomb scattering between the nuclei. Toward the left they gradually depart from the pure Coulomb form in a way that reflects the increasing shielding of the nuclear charges by the electron clouds.

The simplest functional form that can be applied to data of this sort is the exponentially shielded Coulomb potential originally used by Bohr:

$$V_B=(\zeta e^2/c)\ (c/r)\exp(-r/c); \tag{14}$$

the constant ζ according to the simple theory should be equal to the product of the nuclear charges

$$\zeta=Z_1Z_2, \tag{15}$$

and according to Bohr the screening length is given by

$$c_B=a_0[Z_1^{2/3}+Z_2^{2/3}]^{-1/2}. \tag{16}$$

However, the potential of Eq. (14) can be treated as a two-parameter function with the constants ζ and c to be evaluated by making the best fit to the experimental results. It is easy to do this using the reduced functions ρ versus τ appropriate to the exponentially screened Coulomb potential tabulated in Ref. 5. When this is done, we find the following values of ζ and c:

He^++Ne:

$c_{Ne}=0.68\pm0.04$ atomic unit (a.u.) $=0.36\pm0.02$ Å,

$\zeta_{Ne}=17.5\pm1$.

He^++Ar:

$c_{Ar}=0.80\pm0.06$ a.u. $=0.425\pm0.03$ Å,

$\zeta_{Ar}=30\pm2$.

The values of ζ are obtained mainly through fitting the high-energy data. The values of c are obtained by requiring the curve to go through the low-energy data of Lorents and Aberth; for this purpose the fit was made directly to the corrected calibration data of Figs. 1 and 2. The resulting curves are those marked 1 in Figs. 1 through 4.

Many authors have attempted to improve upon the simple exponentially shielded Coulomb potential by

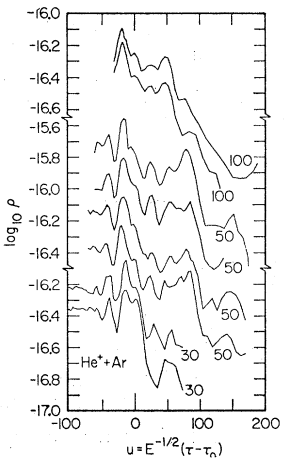

FIG. 8. He^++Ar. Details of the curve-crossing perturbation plotted in the variable u instead of τ to show the proper scaling of the interference oscillations; individual runs are shown separately. The scales on the left apply to the lowest curve at each energy; the upper curves for 30 and 100 eV are displaced by 0.1 unit, and those for 50 eV are displaced by by 0.2 unit.

making use of the modified shielding function derived from the Thomas-Fermi statistical model for the electron clouds. This potential,

$$V_{TF}=(\zeta e^2/c)\ (c/r)f_{TF}(r/c) \tag{17}$$

(where f_{TF} is a tabulated function[10]), can also be treated as a two-parameter function and the reduced cross section computed for it. If that is done, it turns out to deviate very little from the reduced cross section for the case of simple exponential shielding except at small values of τ, where the Thomas-Fermi function behaves as shown in the curve marked T–F in Fig. 1. This behavior is related to the known deficiencies of the statistical model in the outer part of the atom. The Thomas-Fermi function therefore gives no significant improvement in fitting the experimental results, as far as the shape of the function is concerned.

With regard to the shielding constant c, however, several choices have been suggested in addition to a purely empirical fit. Firsov[11] has introduced a formula different from Bohr's to be used in connection with the Thomas-Fermi function:

$$c_F=0.8853a_0[Z_1^{1/2}+Z_2^{1/2}]^{2/3}. \tag{18}$$

When Lane and Everhart computed empirical potentials from the scattering data, they observed better agreement with the Thomas-Fermi-Firsov formula (18) than with the Bohr formula; we suspect this to be due mainly to the change in screening lengths rather than to the form of the screening function. More recently Firsov[12] has introduced two further alternatives:

$$c_{F'}=0.8853a_0\times 7Z_1Z_2/3[(Z_1+Z_2)^{7/3}-Z_1^{7/3}-Z_2^{7/3}] \tag{18'}$$

and

$$c_{F''}=0.8853c_B. \tag{18''}$$

Using (16), (18), (18a), and (18b), the various predicted values of c are (in a.u.)

	c_B	c_F	$c_{F'}$	$c_{F''}$
Ar:	0.344	0.279	0.324	0.305
Ne:	0.398	0.321	0.380	0.353

none of which have any pronounced resemblance to the experimental values we have measured here. The great difference between our conclusions and Lane and Everhart's in this regard arises because the evaluation of c is especially sensitive to the low-energy data, which were not available to them.

From the data tabulated above it is evident that the effective value of the product of nuclear charges ζ is significantly smaller, even in the experiments at 100 keV, than the true product of the nuclear charges, which would be 20 for neon and 36 for argon. It is immediately obvious, however, that agreement would be greatly improved if we assume that K-shell shielding is substantially complete in both these cases. In that case, we expect $\zeta_{Ne}=16$, $\zeta_{Ar}=32$.

By comparing Figs. 3 and 4, it is clear that two-parameter potential functions fit the neon data considerably better than the argon data. In the latter case, over a considerable range in τ, Everhart's results fall below the curve 1 by a factor of 2, which is much greater than the apparent internal error in his experimental results. This suggests a different exponential shielding length applicable to the high-energy data from that applying to the low-energy elastic data. A plausible source for this is the existence of separate screening lengths for the L-shell and the M-shell electrons. Assuming this to be the case, we estimated the L-shell screening length from the Everhart data alone and obtained $c_L=0.14$ a.u. The final result for the repulsive potential in argon is then

$$V_{Ar}=\frac{2e^2}{r}[8e^{-r/c_M}+8e^{-r/c_L}+2e^{-r/c_K}]. \tag{19}$$

Since we are unable to evaluate c_K from the data, we have in fact assumed it to be zero and neglected the last term. The best adjustment of the constants is then $c_M=0.90$ a.u., $c_L=0.14$ a.u. Curve 2 in Figs. 2 and 4 shows the fit of this function to the experimental data.

The argon data thus lead unambiguously to a simple shell structure given by Eq. (19). For neon the corresponding potential is

$$V_{Ne}=(2e^2/r)[8e^{-r/c_L}+2e^{-r/c_K}]. \tag{20}$$

The data probably do not really suffice to evaluate c_K reliably in this case, but we obtain a reasonable fit to the Everhart results by assuming $c_K\cong 0.07\pm 0.02$ a.u. A revised fit including this term and a polarization term (see the next section) gives a probable value of $c_L=0.70$ a.u.

Since a shell-structure potential is so insistently demanded by the empirical data, it is natural to compare the screening lengths with the predictions of atomic theory. The effective radius to be associated with each shell is well known to be connected with the ionization potential of that shell (at least approximately) by the simple hydrogenic formulas

$$c_i=(e^2/2I_i)^{1/2};\qquad a_0\approx a_0/Z_i. \tag{21}$$

This enables us to make the comparisons shown in Table I. We can also compare our screening lengths with those obtained in Hartree (or Hartree-Fock) calculations. Byatt has given a useful tabulation of effective

[10] J. Lindhard, M. Scharff, and H. E. Schiøtt, Kgl. Danske Viderskab. Selskab, Mat. Fys. Medd. **33**, No. 14 (1963).

[11] O. B. Firsov, Zh. Eksperim. i Teor. Fiz. **33**, 696 (1957) [English transl.: Soviet Phys.—JETP **6**, 534 (1958)].

[12] O. B. Firsov, Zh. Ekspeirm. i Teor. Fiz. **34**, 447 (1958) [English transl.: Soviet Phys.—JETP **7**, 308 (1958)].

TABLE I. Shell-structure shielding lengths.

Element	Shell	I (eV)	$(e^2/2I)^{1/2}$ (a.u.)	a_0Z_i	c_{expt} (a.u.)	Hartree-type calculations (a.u.)
Ar	M	$15.755(I_1)$	0.93	1	0.90	0.588,[a,b] 0.596[a,c]
	L	$422.6(I_9)$	0.18	0.111	0.14	0.122,[a,b] 0.104[a,c]
	K	$4115(I_{17})$	0.057	0.059	...	... ...
Ne	L	$21.559(I_1)$	0.79	1	0.70	0.420[a]
	K	$1195.4(I_9)$	0.107	0.111	0.07(±0.02?)	...

[a] William J. Byatt, Phys. Rev. 104, 1298 (1956).
[b] A. E. Ruark, Phys. Rev. 57, 62 (1940).
[c] J. Holtzmark, Z. Physik 55, 437 (1929); 66, 49 (1930).

screening constants from Hartree-type calculations, which we have used in the table.

B. Discussion

The 2-term screened-Coulomb functions we have been led to are clearly only an approximation to the true interactions responsible for the observed scattering. They are, however, extremely valuable because of the ease with which they can be generalized to apply to other cases of scattering of light ions (or atoms) by heavy ones. One condition that clearly must be fulfilled is that the light projectile must either be fully ionized or be approaching with sufficient energy to strip off its remaining electrons before it is significantly deflected from its initial course. In that case the projectile nucleus may act essentially as a Coulomb probe mapping the field in the inner core of the target atom. If the projectile's nuclear charge is Z_1, the target's is Z_2, and the electron-density distribution in the unperturbed target is $\rho_{el}(r)$, the potential governing the nuclear motion can then be approximated by

$$V(r)=Z_1Z_2(r)e^2/r, \tag{22}$$

where

$$Z_2(r)=Z_2-4\pi\int_0^r r^2\rho_{el}(r)\,dr. \tag{22'}$$

Obviously such an approximation can only work if Z_1/Z_2 is small; otherwise $\rho_{el}(r)$ would be too greatly modified in going from the atom Z_2 to the united atom with $Z_2'=Z_1+Z_2$. It should quite generally be possible to approximate (22) further by a sum of exponentially shielded terms.

3. Rainbow Scattering and the Attractive Potential

For He^++Ar the reduced cross section shows a clear indication of the sharp rise at small reduced angles that is typical of the rainbow behavior due to an attractive well in the potential. This feature occurs at a rainbow angle of about $\tau_r=32$ eV deg. Associated with this structure at somewhat larger reduced angles, the reduced cross section shows clear signs of falling below the curve calculated from the screened Coulomb repulsive potential. Indeed, over a considerable range the reduced cross section is essentially horizontal. A similar horizontal region is seen in the data for He^++Ne, but no rainbow structure in the region accessible to measurement. However, the fact that the experimental curve falls below the screened Coulomb one is a clear indication of the occurrence of an attractive term in the potential.

The most obvious source for attractive forces is the polarization of the target atom by the approaching ion. Formally, a simple polarization term with its r^{-4} dependence has an embarrassing singularity at the origin. Physically, however, the dominating contribution to the polarization is due to the outermost shell of electrons in the atom and must fade away as the approaching ion passes through this shell. It seems appropriate therefore to represent the complete polarization term by a function which has the proper r^{-4} behavior at large distances and which is exponentially damped to at most a constant limit as $r\to 0$. The appropriate screening length for this exponential damping would clearly be identical with the screening constant for the outermost electron shell. It is therefore possible to introduce such a screened polarization term with only a single new constant, namely, the polarizability. The simplest form that avoids the singularity of the origin is

$$V_{pol}=-(\alpha e^2/c^4)x^{-4}[1-e^{-x}(1+x+\tfrac{1}{2}x^2+\tfrac{1}{6}x^3)], \tag{23}$$

where $x=r/c$. This screened polarization term is similar in form to one previously used by Temkin in the problem of e–H scattering.[13]

In order to compute the reduced scattering functions appropriate to this term in the potential, some additional analysis must be performed. This is done in the Appendix, where we show that all functions of this type can be handled by using tabulated Bessel functions and their integrals. It is therefore a simple matter to fit the experimental curve by using the polarizability as an adjustable parameter. This fit can be carried out in 2 ways, by adjusting either to the reduced rainbow angle or to the horizontal part of the reduced cross section (see Appendix). In the case of He^++Ar the polariza-

[13] A. Temkin, Phys. Rev. 116, 358 (1959); A. Temkin and J. C. Lamkin, *ibid.* 121, 788 (1961).

TABLE II. Polarizability.

	α_r (Å^3)	α_{dev} (Å^3)	α_{calc} (Å^3)	τ_r (eV deg)	b_r/a_0	r_{min}/a_0	V_{min} (eV)
Ar	1.85	1.65±0.10	1.64	32	6.6	5.7	−0.146
Ne	...	0.41±0.04	0.395	(4.6)[a]	6.1	5.4	−0.047

[a] Predicted.

bility required for these two adjustments agrees within 10%. This gives us considerable confidence that the postulated potential is really of the correct shape. (We have in fact tried a different shape, namely, a pure exponential attraction added on to the screened Coulomb repulsion, and we find that it is impossible to fit both features of the experimental curves even by allowing the exponential constant to vary as well as the pre-exponential magnitude.) In the case of He^++Ne only one method of fitting the polarizability is available to us, namely, adjustment to fit the horizontal portion of the curve. In Table II we report the resulting values we obtained for the polarizabilities of Ne and Ar and we compare them with Dalgarno's[14] calculated values. The agreement is most gratifying. The table shows the depth and location of the minimum calculated from the postulated potential.

We have included in Table II an estimate of the magnitude of the error in the polarizability. It should be pointed out that this constant occurs in the dimensionless combination

$$B=\alpha/16c^3 \tag{24}$$

in making the fit to the experimental results. The polarizability therefore depends very strongly on possible errors in the screening constant for the outer shell, and the agreement with Dalgarno's values for α implies a strong confirmation of the accuracy of the screening constants.

It is a matter of considerable surprise to us to find that the elastic-scattering data can be reproduced so well by so simple a potential as we have introduced, namely, a combination of a screened-Coulomb repulsion with a screened polarization attraction, and that the adjustable constants, the screening constants and the polarizability, agree so well with expectation. We can only conclude that additional contributions to the potentials will be comparatively small.

4. Curve Crossings

Obviously, not all of the bumps seen on the cross-section curves are meaningful, and many of them merely represent residual noise. However, those features which occur at approximately the same value of τ can be expected to be real. Scattering effects are particularly sensitive to features of the interaction potential near the classical distance of closest approach, since the radial motion of the nuclei is slowest at this point and thus the time available for the perturbing forces to act is longest. Because constant τ implies constant b and r_0, it is possible to identify a feature in the data at some τ with a feature of the potential at some value of the internuclear separation. Such a feature is evident in the data in Figs. 3 and 5 at $\log_{10}\tau\cong 3.2$ and in Figs. 4 and 6 at $\log_{10}\tau\cong 2.8$, where a series of pronounced oscillations are seen to begin and die off to the right. We have already suggested that these oscillations are a perturbation of the elastic-scattering pattern due to the crossing of two potential-energy curves.[15]

The elastic scattering of course is dominated by the molecular-state dissociating to the ground states of the ion He^+ and the target atom (Ne or Ar). The perturbing state in the crossing probably dissociates to ground-state He^+ and the first excited state of Ne or Ar, although other low-lying excited states are possible candidates. From our knowledge of the potentials for the elastic scattering we are able to relate the value of τ at the crossing to the impact parameter and the distance of closest approach and thus to estimate the location of the first observed curve crossing. From the position of the major peak we locate this crossing near $2.0a_0$ in He^++Ne and near $3.1a_0$ in He^++Ar.

The perturbations in question show several distinctive features. As τ increases past some threshold value, we see first a pronounced dip in the reduced cross section and then a rise to a peak which considerably exceeds the extrapolated smooth cross-section curve. Following this rise the curve falls more or less to its previous height and shows a continuing series of more or less regular oscillations which gradually fade out or merge into further structure due to other interactions. These oscillations we believe to be due to an interference effect representing the fact that there are two possible trajectories for the elastic-scattering collisions when the impact parameter is smaller than the crossing distance r_x. A pure elastic trajectory T_I corresponds to the basic diabatic potential curve dissociating smoothly to the initial atom and ion states. A second elastic trajectory T_{II} is possible if a transition occurs to the excited-state curve when the system passes inward at r_x and a second transition back to the ground-state curve occurs on the subsequent outward passage. In the latter case the turning point

[14] A. Dalgarno and A. E. Kingston, Proc. Roy, Soc. (London) **A259**, 424 (1960).

[15] F. T. Smith, D. C. Lorents, W. Aberth, and R. P. Marchi, Phys. Rev. Letters **15**, 742 (1965).

TABLE III. Parameters of the curve crossing.

	τ_x (eV deg)	r_x (a.u.)	L (a.u.)
Ne	1950	1.9	1.6
Ar	870	2.9	1.9

for the collision is determined by the excited-state curve which lies below the ground-state curve inside r_x. Because of the existence of these two possible trajectories, the scattering amplitude at a given angle θ will contain two components which will interfere to give the oscillating pattern. A similar feature is seen in the inelastic-scattering pattern attributed to a curve crossing of a nature very similar to this one.

The major peak in the perturbation is much larger than any of the others and appears to represent more than just the first peak in a smoothly varying interference pattern. In fact, that interference pattern is under ordinary circumstances expected to fall below the extrapolated smooth elastic cross section and not to rise much above it. However, if the excited potential curve in the crossing is strongly attractive and has a potential minimum near or inside r_x, the second trajectory may involve a cross section which displays the effect of this attractive well in a manner similar to the rainbow maximum seen in the ordinary scattering due to a simple attractive potential. We are inclined to believe that such a rainbow feature is the explanation for the very large rise seen here. In the analogous case of He^++He the adiabatic potential curves calculated by Michels[16] and by Browne[17] show a pseudocrossing involving an interaction between a very strongly attractive state with a minimum inside the crossing and a pure repulsive state dissociating to the ground-state ion-atom pair. On chemical grounds we believe a similar strongly attractive curve will be formed when He^+ approaches singly excited Ne or Ar.

On the basis of a simple semiclassical theory it is possible to give a somewhat more detailed analysis of the curve-crossing perturbation. The oscillatory interference pattern due to the two competing trajectories labeled I and II gives rise to a term in the cross section proportional to $\cos 2\pi N(\tau, E)$. The index N is related to the difference in classical action integrals A over the two trajectories and to the reduced classical action a by the equation

$$vhN(\tau, E) = v\Delta A(\tau, E) = v[A_{\mathrm{I}}(\tau, E) - A_{\mathrm{II}}(\tau, E)] = \Delta a(\tau, E) = \Delta a_0(\tau) + E^{-1}\Delta a_1(\tau) + \cdots . \quad (25)$$

An approximate method of analyzing the scattering is obtained if we divide this equation by the velocity v and define the variables

$$t = E^{-1/2}\tau = u + E^{-1/2}\tau_x,$$
$$u = E^{-1/2}(\tau - \tau_x) = t - E^{-1/2}\tau_x. \quad (26)$$

These variables are the natural ones to use if the functions on the right-hand side of Eq. (25) are expanded about some point τ_x. It is natural to take this point as the true crossing threshold where the two trajectories merge so that

$$\Delta a_0(\tau_x) = 0. \quad (27)$$

As the energy is varied, the oscillations remain in phase when N is constant; this is roughly equivalent to the condition that u be constant.

In Figs. 7 and 8 we show the reduced cross sections for a number of runs plotted against the variable t or u. We include several separate runs at various energies in order to show the reproducibility of the patterns. This is sufficiently good to make possible the detection of errors in the angular measurement which may be due either to inaccurate alignment or to stray electrostatic fields. In the case of the data at 50 eV for He^++Ar, a discrepancy of close to 1° in the angular measurement was observed; the curves as shown in the figure have been shifted to coincide and the average angle was used to compute u. In the case of He^++Ne at 150 eV, it appears from Fig. 7 that a small angular correction would be appropriate.

It is clear from Figs. 7 and 8 that the individual peaks in the scattering pattern can be unambiguously identified with each other as the energy is changed, even though the absolute numbering system for N is uncertain. It is thus possible to plot the motion of a single peak in the variable t as a function of the variable $E^{-1/2}$. By Eq. (26) the slope of this curve measures τ_x, the true crossing threshold. [A more detailed analysis based on an expansion of Eq. (25) confirms this conclusion.] By means of such an analysis we have located the threshold value τ_x and the corresponding crossing point r_x from the experimental data; the results are given in Table III. These values of τ_x have been used to establish the variable u used in Figs. 7 and 8.

It is significant that the oscillations extend on both sides of the apparent threshold τ_x; this behavior as well as the enhanced, rainbowlike, maximum to the left of τ_x is to be expected because of the shape of the deflection functions and phases associated with the two interfering trajectories I and II (which we hope to discuss more thoroughly elsewhere). The spacing of these oscillations is a significant parameter, conveniently expressed in terms of a length by means of a relation derived from (25) and (26):

$$L = d\Delta a_0/d\tau = (2/\mu)^{1/2}hdN/du. \quad (28)$$

The spacing is seen to increase (and L to decrease) gradually as u increases; we give an average value in Table III. This quantity depends largely on the

[16] H. H. Michels (private communication).
[17] J. C. Browne, J. Chem. Phys **45**, 2707 (1966).

difference potential $\Delta V(r)$ near r_x. The amplitude of the oscillations, on the other hand, depends both on the difference potential and on the coupling energy $H_{12}(r_x)$; more detailed measurements may make it possible to deduce H_{12} and then to predict the inelastic cross sections associated with the perturbation. It is already obvious that the amplitude of the perturbation is much greater in Ar than in Ne, though we cannot yet be sure whether this arises primarily from differences in H_{12} or in $\Delta V(r)$.

There remains some additional movement of the peaks in Figs. 7 and 8 as a function of energy. This is not surprising in view of additional energy-dependent terms in Eq. (25), but these shifts are rather small and we shall not attempt to analyze them here. They may, however, eventually provide additional information on the interactions.

Before leaving this section, it is worth remarking that the regular oscillations associated with this single curve crossing appear to be responsible for almost all of the structure that can be clearly observed up to the point where the steep elastic loss (to be discussed in the next section) sets in. This must indicate that the curve crossings are widely separated, or else that the interactions H_{ij} coupling the two states involved in other crossings are in most cases too small to yield easily observable perturbations.

5. The Elastic Loss in Close Encounters

One of the most striking features of the elastic-scattering data at fairly large values of τ is the great drop in the reduced cross section that occurs in both He^++Ne and He^++Ar. This precipitous fall comes at the same location and with the same shape and abruptness at all energies, except for some details of structure appearing in the final region of very low cross section. Clearly, the severe drop reflects a mechanism providing extensive losses into one or more inelastic channels.

Knowing the potentials for pure elastic scattering, it is a simple matter to compute the fraction remaining in the elastic channel, and thus the fraction lost, as a function of the reduced angle τ or the impact parameter b. Since we are dealing with losses in large-angle scattering we have, where needed, used two terms of the impact expansion to make the evaluation:

$$P_{el}(\tau, E) = [\rho_{expt}(\tau, E)/\rho_0(\tau) + E^{-1}\rho_1(\tau)], \qquad (29)$$

where ρ_0 and ρ_1 were computed from the approximate potentials. We have also computed the impact parameter,

$$b(\tau, E) = b_0(\tau) + E^{-1}b_1(\tau), \qquad (30)$$

so as to plot $1-P_{el}(\tau, E)$ versus b^2. Since we only used the one-term screened Coulomb potential to compute ρ_1 and b_1, the results of this section are only semi-quantitative.

An examination of these plots shows that $P_{el}(\tau, E)$ depends very little on E, and except for minor details it is a very simple function of τ. At small τ, P_{el} is unity; after the first curve-crossing perturbations it may fall somewhat, but not very much, below unity. At a certain point, however, P_{el} begins to drop essentially linearly with b^2, and does so until it flattens out at a rather constant value that is a small fraction of its initial magnitude. Within the accuracy of our measurements, both the location of the midpoint and the width (or slope) of this drop are independent of the energy, and the mean value of the ultimate P_{el} attained after the drop is very small except at the lower energies. It is very important that the width $\Delta\tau_d$ or Δb_d of this drop is energy-independent, since this implies that it is not limited by the angular resolution of the measurements. (If they were resolution-limited, $\Delta\theta$ would be constant and $\Delta\tau$ would vary as $1/E$; the observations show no such trend.) Both the location and the width thus measure features of the interaction. We give the results both in terms of the measured quantity τ and the derived one b, the latter representing essentially the classical turning point r_0 and therefore the location of the interaction on a potential diagram; the widths are full widths, not half-widths.

	τ_d (eV deg)	$\Delta\tau_d$ (eV deg)	b_d (a.u.)	Δb_d (a.u.)
Ne	6000±500	7000±1000	1.23	0.32
Ar	2000	2000	2.16	0.55

In at least two ways this loss phenomenon differs from the usual curve-crossing perturbation. First, its width appears to be greater, and second there is no recovery from it once the critical region of impact parameter is passed. Both of these features imply an interaction of different magnitude and perhaps of different type from the simple curve crossing.

The usual curve crossing is characterized by the existence in some simple approximation of two molecular states whose interaction $|H_{12}|$ is everywhere smaller than their separation $|V_{11}-V_{22}|$ except accidentally in a restricted region where they approach closely or cross; consequently, the two states are well defined by the *same* molecular orbital description on both sides of the interaction region. A different and contrasting situation prevails where two states 1 and 2 are well defined and well separated ($|V_{11}-V_{22}| > |H_{12}|$) in one region (say, $r \geq R$), but H_{12} becomes greater than their separation for all of another large region (say, $r \leq R$). In the latter case it may be possible to change the description of the states, and define new combinations (by new approximate symmetries, perhaps) which give a better description in the second region ($|V_{1'1'}-V_{2'2'}| < |H_{1'2'}|$ for $r \leq R'$). This may be called an extended-coupling situation in contrast to the restricted coupling of the curve crossing. As an example, consider the collision of two atoms each initially in a doublet state, but with a possible quartet excited state.

From these can be constructed molecular singlet and triplet states. When r is large, the description in atomic states is appropriate, and when it is small the molecular description must be preferred.

In the case at hand, we believe that a situation of extended coupling at small r may connect the incoming state $He^+ + Ar$ with one or more states of the dissociated form $He + Ar^+$; at small r the description in terms of ion-atom pairs is inappropriate, and recourse must be had to a molecular or even a united-atom description with contributions of approximate g and u symmetry. In view of the great difference between these two descriptions, it would not be surprising to find the incoming state $He^+ + Ar$ decomposing into a set of several g and several u united-atom states—and each of these in turn dissociating to a mixture of several states of $He^+ + Ar$ and several states of $Ar^+ + He$, and perhaps some multiply ionized states in addition. Once the region of united-atom coupling has been entered, the phase of each of the contributing states will change in its own way as a function of τ and E, and when the particles separate again the new mixture of phases will usually not interfere constructively so as to reconstitute the initial incoming state but rather lead to a complicated mixture of the various dissociating states participating in the united-atom set. On the average, then, P_{el} will approach $1/N$, where N is the number of dissociating states, or channels, participating. $P_{el}(\tau, E)$ will still deviate from its average value from place to place, but less often and less far as N increases. As far as we can tell, this description applies very well to the behavior of P_{el} as we observe it after the falloff is passed; the occasional deviations of P_{el} from its average trend may be responsible for the rather irregular structure seen in Figs. 3 and 4 to the right of the principal drop. The resulting average value of $P_{el}(\tau, E)$ can then be used to estimate the number N of channels participating in the extended-coupling set, and we can also try to see whether N varies significantly with E.

Clearly the mean impact parameter b_d of the falloff pattern approximately measures the location r_d where two or more states of the separated-atom description become severely mixed with each other. The width Δb_d of the pattern is as yet not so easy to interpret, but it is obviously an important observable and closely connected with the behavior of the states in question. Since we know the elastic potential $V(r)$ and its derivative $V'(r)$, we can tentatively translate Δb_d to an energy by the formula

$$\Delta U_d = \Delta b_d V'(r_d). \tag{31}$$

The result is $\Delta U_d(\mathrm{Ne}) = 47$ eV; $\Delta U_d(\mathrm{Ar}) = 25$ eV. We may hope that these quantities afford some crude measure of the magnitude of the coupling that mixes the various states in the extended-coupling set.

An additional feature of the strong-coupling situation can be seen in Fig. 4, where it appears that the extent of the drop in cross section increases with the energy of the collision, varying from a factor of about 5 to a factor of perhaps 30. If this ratio is indeed a measure of the number N of channels participating in the inelastic process, it would appear that the coupling itself is strongly energy-dependent. This would not be surprising, since the mixing is expected to extend over a wider band of states when the collision duration is shorter, mainly as a result of the uncertainty principle. Clearly there is in this phenomenon much material for further investigation.

As far as the elastic channel is concerned, the loss process occurring here could be treated by a simple absorption model. Clearly, diffraction effects should be connected with the scattering at the edge of the loss region, and a simple calculation suggests that they could be observed by careful measurements with presently attainable resolution. By analogy with the simple case of an absorbing disk, one expects the spacing of the diffraction peaks to be given by the approximate formula

$$kR\Delta\theta \approx \pi, \tag{32}$$

where R is the radius of the absorber. Thus, if $\Delta\theta$ is in degrees, we find

$$\Delta\theta \approx 1.1(R/a_0)\,(100\ \mathrm{eV}/E)^{1/2}, \tag{33}$$

which indicates that these oscillations will have a period of the order of 1° or slightly less. It is interesting to note that in the case of $He^+ + Ar$ there appears to be a rise in the reduced cross section just to the left of the strong absorption; this is seen in several curves in Figs. 6 and 8. Such a rise is a common occurrence in nuclear scattering at the onset of a strong absorption.[18]

V. CONCLUSION

We began the work presented in this paper with the modest aim of testing the scaling principle derived from the semiclassical theory of small-angle scattering. The phenomena so revealed tempted us inductively into the more thorough analysis that we have presented here. The results have convinced us of the feasibility of interpreting differential scattering data in a spectroscopic manner to deduce potentials and interactions between electronic states from the details of the experimental scattering patterns. Among other things, this work has demonstrated the advantages of using data over a very wide span in energy. It has also convinced us of the feasibility of interpreting inelastic processes, such as those associated with curve crossings, in addition to the simple elastic potential scattering.

APPENDIX

1. Screened Power-Law Potentials

When the potential is a power law, a simple exponential, or an exponentially screened Coulomb law, the

[18] See, for example, John S. Blair, in *Lectures in Theoretical Physics* (University of Colorado Press, Boulder, Colorado, 1966), Vol. VIII-C, pp. 343–444.

integrals appearing in the forward impact expansion can be evaluated with the use of functions no more complicated than the modified Bessel functions K_0 and K_1. Similar forms result if the potential is a product of an exponential and a polynomial. One further form of integral must be available if long-range attractive forces are to be treated realistically by allowing them to be exponentially damped as $r\to 0$. The damped polarization potential is an example:

$$V_{\text{pol}}=-\frac{\alpha e^2}{r^4}\left[1-e^{-r/c}\left(1+\frac{r}{c}+\frac{r^2}{2c^2}+\frac{r^3}{6c^3}\right)\right]; \quad \text{(A1)}$$

at the origin this approaches the value $V_{\text{pol}}(0)=-\alpha e^2/24c^4$, instead of diverging. In handling this type of potential we encounter integrals of the form

$$g_m(\alpha)=\int_1^\infty x^m e^{-\alpha\rho}(x^2-1)^{-1/2}dx, \quad \text{(A2)}$$

where m is an integer and may be negative. The functions $g_m(\alpha)$ satisfy the recursion relations

$$(m+1)\,g_m=\alpha(g_{m+1}-g_{m+3})+(m+2)\,g_{m+2} \quad \text{(A3)}$$

and

$$\frac{dg_m}{d\alpha}=-g_{m+1}(\alpha), \qquad g_m(\alpha)=\int_\alpha^\infty g_{m+1}(a)\,da. \quad \text{(A4)}$$

For non-negative m's these functions can all be expressed as simple combinations of the Bessel functions K_0 and K_1:

$$\begin{aligned} g_0(\alpha)&=K_0(\alpha),\\ g_1(\alpha)&=K_1(\alpha),\\ g_2(\alpha)&=\alpha^{-1}K_1(\alpha)+K_0(\alpha), \text{ etc.} \end{aligned} \quad \text{(A5)}$$

For negative m's we must use one additional function,

$$g_{-1}(\alpha)=Ki_1(\alpha)=\int_\alpha^\infty K_0(a)\,da. \quad \text{(A6)}$$

This integral is tabulated,[19] and various approximations are also available. With its help and using (A3), we then have

$$\begin{aligned} g_{-2}(\alpha)&=\alpha K_1(\alpha)-\alpha Ki_1(\alpha),\\ g_{-3}(\alpha)&=\tfrac{1}{2}(\alpha^2+1)Ki_1(\alpha)+\tfrac{1}{2}\alpha K_0(\alpha)-\tfrac{1}{2}\alpha^2K_1(\alpha),\\ g_{-4}(\alpha)&=-\tfrac{1}{6}\alpha(\alpha^2-3)Ki_1(\alpha)-\tfrac{1}{6}\alpha^2K_0(\alpha)\\ &\quad+\tfrac{1}{6}\alpha(\alpha^2+4)K_1(\alpha). \end{aligned} \quad \text{(A7)}$$

When m is negative, g_m goes to a finite limit at 0:

$$g_{-n}(0)=\Gamma(\tfrac{3}{2})\Gamma(\tfrac{1}{2}n)/\Gamma(\tfrac{1}{2}(n+1)), \qquad n>0. \quad \text{(A8)}$$

[19] *Handbook of Mathematical Functions*, edited by M. Abramowitz and I. Stegun, (U.S. Department of Commerce, National Bureau of Standards, Washington, D.C., 1954) Appl. Math. Ser. No. 55, pp. 492 ff.

In dealing with the leading term of the impact expansion for the reduced scattering angle $\tau(b)$ and the reduced cross section $\rho(\tau)$, we encounter the integrals

$$\begin{aligned} t_m(\alpha)&=-\int_1^\infty \frac{d}{dx}(x^m e^{-\alpha x})(x^2-1)^{-1/2}dx\\ &=\alpha g_m(\alpha)-mg_{m-1}(\alpha) \end{aligned} \quad \text{(A9)}$$

and its derivative

$$dt_m/d\alpha=-t_{m+1}(\alpha). \quad \text{(A10)}$$

Using (A3) we find

$$t_m(\alpha)-t_{m-2}(\alpha)=-g_{m-1}(\alpha). \quad \text{(A11)}$$

From these it is easy to evaluate the specific cases

$$\begin{aligned} t_1(\alpha)&=\alpha K_1(\alpha)-K_0(\alpha),\\ t_0(\alpha)&=\alpha K_0(\alpha),\\ t_{-1}(\alpha)&=\alpha K_1(\alpha),\\ t_{-2}(\alpha)&=\alpha K_0(\alpha)+Ki_1(\alpha),\\ t_{-3}(\alpha)&=2\alpha K_1(\alpha)-\alpha Ki_1(\alpha),\\ t_{-4}(\alpha)&=\tfrac{1}{2}(\alpha^2+3)Ki_1(\alpha)+\tfrac{3}{2}\alpha K_0(\alpha)-\tfrac{1}{2}\alpha^2K_1(\alpha). \end{aligned} \quad \text{(A12)}$$

At the origin we have

$$t_{-n}(0)=\Gamma(\tfrac{1}{2})\Gamma(\tfrac{1}{2}(n+1))/\Gamma(\tfrac{1}{2}n), \qquad n>0. \quad \text{(A13)}$$

It is also useful to define

$$s_m(\alpha)=\alpha^m t_m(\alpha), \quad \text{(A14)}$$

whose derivative is given by

$$-\alpha s_m'(\alpha)=s_{m+1}(\alpha)-ms_m(\alpha). \quad \text{(A15)}$$

These functions can be used to evaluate the reduced scattering angle

$$\tau_0(b)=-b\int_b^\infty \frac{dV}{dr}(r^2-b^2)^{-1/2}dr \quad \text{(A16)}$$

and the reduced cross section

$$\rho_0(b)=|\,b\tau_0(b)/\tau_0'(b)\,| \quad \text{(A17)}$$

for a broad class of potentials $V(r)$. If we write the potential as

$$\begin{aligned} V(r)&=\sum_m[A_m r^m+\sum_i a_{mi}(r/c_i)^m e^{-r/ci}]\\ &\qquad (A_m=0 \text{ for } m\geq 0), \end{aligned} \quad \text{(A18)}$$

we can include both power-law and exponential terms. With this potential, it follows that

$$\tau_0(b)=\sum_m[A_m b^m t_m(0)+\sum_i a_{mi}s_m(b/c_i)] \quad \text{(A19)}$$

and

$$\tau_0'(b)=\sum_m[mA_m b^{m-1}t_m(0)+\sum_i(ma_{mi}-a_{m-1,i})b^{-1}s_m(b/c_i)]. \quad \text{(A20)}$$

In the particular case of the polarization potential (A1), we have

$$(c^4/e^2\alpha)\tau_0(b;V_{\rm pol})=s_{\rm pol}(\beta)$$
$$=\tfrac{1}{2}\beta^{-4}[-\tfrac{3}{2}\pi+3Ki_1(\beta)+(3+\beta^2)\beta K_0(\beta)+(3+\beta^2/3)\beta^2K_1(\beta)], \quad \text{(A21)}$$

where $\beta=b/c$. The first derivative is

$$-(c^5/e^2\alpha)\tau_0'(b)=-s_{\rm pol}'(\beta)=\beta^{-1}[4s_{\rm pol}(\beta)+\tfrac{1}{6}\beta K_0(\beta)]. \quad \text{(A22)}$$

As long as the potential has the general form (A16), all the higher terms of the forward impact expansion for both the scattering angle and the classical action can be obtained in a similar way with the use of the same tabulated integrals (A5) and (A6). For example, if the potential is

$$u_m(x)=x^me^{-x}, \quad \text{(A23)}$$

the reduced classical action has as its leading term a new function $q_m(\beta)$ defined by

$$\alpha_0=q_m(\beta)=m\beta^{m+1}g_{m+1}(\beta)-\beta^{m+2}g_{m+2}(\beta). \quad \text{(A24)}$$

2. Fitting the Attractive Potential

The potential is fitted in the form

$$u(x)=cV(x)=u_{\rm rep}(x)+Bu_{\rm pol}(x), \quad \text{(A25)}$$

where

$$u_{\rm rep}(x)=x^{-1}[e^{-x}+\Gamma e^{-\gamma x}], \quad \text{(A26)}$$

$$u_{\rm pol}(x)=-x^{-4}[1-e^{-x}(1+x+\tfrac{1}{2}x^2+\tfrac{1}{6}x^3)], \quad \text{(A27)}$$

$$x=r/c, \qquad \beta=b/c, \qquad B=\alpha/16c^3, \quad \text{(A28)}$$

and Γ, γ, and c are chosen to fit the 2 cases, Ar and Ne: $c_{\rm Ar}=c_M({\rm Ar})$, $c_{\rm Ne}=c_L({\rm Ne})$, $\gamma_{\rm Ar}=c_M/c_L$, $\gamma_{\rm Ne}=c_L/c_K$, $\Gamma_{\rm Ar}=1$, $\Gamma_{\rm Ne}=\frac{1}{4}$. The corresponding reduced scattering angle is

$$c\tau(b)/16e^2=s(\beta)=s_{\rm rep}(\beta)+Bs_{\rm pol}(\beta), \quad \text{(A29)}$$

where

$$s_{\rm rep}(\beta)=s_{-1}(\beta)+\gamma\Gamma s_{-1}(\gamma\beta). \quad \text{(A30)}$$

B_r, the rainbow value of B, and the associated value of the reduced impact parameter β_r can be deduced from the reduced rainbow angle by the conditions

$$s'(\beta_r)=0, \qquad s(\beta_r)=s_r=c\tau_r/16e^2. \quad \text{(A31)}$$

$B_{\rm dev}$ is the value of B estimated from the observed deviation of the curve $\rho(\tau)$ from the pure repulsive curve derived from (A30). As a result of this deviation, ρ is essentially horizontal over a considerable range in τ. If this constant value is ρ_*, and the horizontal portion intersects the pure repulsive curve at τ_* where $b=b_*$, we can integrate Eq. (A17) from τ_* to τ:

$$\tau_{\rm hor}(b)=\tau_*\exp[(b_*^2-b^2)/2\rho_*], \qquad \tau\leq\tau_*. \quad \text{(A32)}$$

The deviation function is then

$$\tau_{\rm dev}(b)=\tau_{\rm rep}(b)-\tau_{\rm hor}(b); \quad \text{(A33)}$$

over a considerable region in b this proved to be an almost constant multiple of $t_{\rm pol}(\beta)$; the ratio of the two allows us to estimate $B_{\rm dev}$.